PCCP

Accepted Manuscript

ROYAL SOCIETY OF CHEMISTRY

www.rsc.org/pccp

PCCP

RSCPublishing

ARTICLE

Superhydrophobic Ag nanostructures on polyaniline membranes with strong SERS enhancement

Cite this: DOI: 10.1039/xoxxooooox

Weiyu Liu, Peng Miao, Lu Xiong, Yunchen Du, Xijiang Han* and Ping Xu*

Received ooth January 2012,
Accepted ooth January 2012

DOI: 10.1039/xoxxooooox

www.rsc.org/

We demonstrate here a facile fabrication of n-dodecyl mercaptan-modified superhydrophobic Ag nanostructures on polyaniline membranes for molecule detection based on SERS technique, which combine superhydrophobic condensation effect and high enhancement factor. It is calculated that the as-fabricated superhydrophobic substrate can exhibit a 21-fold stronger molecule condensation, and thus further amplify the SERS signal to achieve more sensitive detection. Detection limit of a target molecule, methylene blue (MB), on this superhydrophobic substrate can be 1 order of magnitude higher than that on the hydrophilic substrate. With high reproducibility, the feasibility of using this SERS-active superhydrophobic substrate for quantitative molecule detection is explored. Partial least squares (PLS) model was established for the quantification of MB by SERS, with a correlation coefficient R^2=95.1% and root-mean-squared error of prediction (RMSEP)=0.226. We believe this superhydrophobic SERS substrate can be widely used in trace analysis due to its facile fabrication, high signal reproducibility and promising SERS performance.

Introduction

Surface enhanced Raman scattering (SERS) is a phenomenon whereby the electromagnetic field, at the close proximity of rough metal nanostructure, is locally enhanced because of the resonant interaction with the surface plasmons in the metal.[1, 2] Due to its high sensitivity and spectroscopic precision, SERS has been recognized as a powerful probe for trace detection of chemical and biological molecules in the fields of food safety, environmental and biomedical sciences.[3-5] One of the key issues for the practical applications of SERS is the preparation of active substrates with high enhancement factor, good stability and reproducibility. To date, various SERS substrates have been reported, including roughened silver electrodes, metal nanoparticle assemblies, and even semiconductor-based substrates.[4, 6-11] Notably, most of these fabricated substrates are hydrophilic during SERS measurement.

Recently, it is reported that superhydrophobic substrates have unique advantage in sensing highly diluted and small-volume analytes, especially when sample availability is inadequate or safety issues may arise from the handling of large sample volumes.[12-15] One characteristic of superhydrophobic surface is that it can dramatically reduce the contact area between the droplet and the underlying surface. Therefore, diluted analyte in the droplet can be highly concentrated after its evaporation on the superhydrophobic surface. This condensation effect may further amplify the SERS signal to achieve more sensitive detection. Combination of superhydrophobic substrate and high-sensitivity plasmonic devices has been reported as SERS active substrate due to their high enhancement abilities. For example, superhydrophobic and SERS active device was fabricated by using optical lithography, electron beam lithography and electroless techniques, which can detect rhodamine 6G (R6G) even at atom-molar concentration.[16] Superhydrophobic surfaces with hierarchical micro- and nanoscale surface roughness and hydrophobic chemical functionality, such as lotus,[17] and rose[18] petal-like surfaces, possess superior anti-wetting ability with a water contact angle greater than 150 °. To the best of our knowledge, there have been very limited works reporting the fabrication of superhydrophobic substrates for molecule sensing. Current fabrication of superhydrophobic SERS substrate generally involves two steps: creating a non-metallic superhydrophobic surface with regular geometries, followed by the deposition of metal film and/or nanoparticles to import plasmonic properties to the superhydrophobic surface. Despite the great success of these techniques, characteristics that are too technologically demanding, complex, and expensive restrain their further application in industry level, making SERS detection an "in-lab-only" technique. Quality factor in plasmon resonance, an indication of the strength of surface plasmon resonance, is also expected to be low due to the polycrystallinity of Ag/Au film prepared *via* electroless deposition.[19] Similarly, hydrophobic Teflon film randomly deposited on Ag nanoparticle aggregates can also attain R6G detection at femtomolar level. However, the aggregated Ag nanoparticles may potentially suffer from a structural and SERS signal reproducibility issue. Hence, an appealing superhydrophobic SERS platform is preferably built directly using plasmonic nanostructures that support strong surface plasmon resonance for maximum SERS enhancement.[20]

In our recent works,[21-23] we have shown that rough Ag nanostructures grown on polyaniline (PANI) surfaces as highly efficient and cost-effective SERS platforms can be fabricated through a direct chemical deposition technique, where the size and morphology of the metal nanostructures can be simply controlled by the surface chemistry and chemical nature of

PANI, and other reaction conditions. It has been reported that rough surface can exhibit superhydrophobility through proper chemical modification,[24] and thus multifunctional systems can be obtained with superhydrophobility and promising detection sensitivity. In this article, different from our previous effort to control the size and morphology of Ag nanostructures for SERS applications,[21-23] we demonstrate here a facile method to fabricate superhydrophobic and SERS-active substrate by decorating well-defined Ag nanostructures supported on PANI membranes with n-dodecyl mercaptan. This superhydrophobic substrate shows highly sensitive SERS response to the selected dye target analyte, MB, with a detection limit of 10^{-8} mol/L. Moreover, this substrate with homogeneous Ag nanostructures exhibits high signal reproducibility. The feasibility of using this substrate for quantitative detection *via* partial least-squares (PLS) model was also conducted.

Experimental Section

Materials

PANI emeraldine base (EB) powder (Aldrich), N-methyl-2-pyrrolidone (NMP, 99% Aldrich), heptamethylenimine (HPMI, 98% Acros), $AgNO_3$ (99.9999% Aldrich), lactic acid (Acros), malic acid (Acros), n-dodecyl mercaptan (Aldrich) and hydrazine (Aldrich) were used as received.

Fabrication of PANI Membranes

PANI membranes are fabricated by a phase inversion method using water as the coagulation bath.[25] In a typical experiment, 1.15 g of PANI (EB) powder, 4.14 g of NMP, and 0.747 g of HPMI were mixed in a 12 mL Teflon vial. The mixture was stirred for 0.5–1 h to form a homogeneous solution, followed by being poured onto a glass substrate and spread into a wet film using a gardener's blade with a controlled thickness. The wet film was then immersed into a water bath and kept in the water bath for at least 24 h. The resulting membrane was then dried at room temperature for 6 h, and then cut into 5 mm × 5 mm pieces. The PANI pieces were immersed in 20% hydrazine for 30min before being used for Ag growth.

Growth of Ag Nanostructures on PANI Membranes

The growth of Ag nanostructures on a PANI surface was conducted as follows: one piece of undoped PANI membrane was immersed in a mixture solution of 1 mL of 1 mol/L $AgNO_3$ aqueous solution and 0.1 mL of 0.25 mol/L lactic acid for 30 min. After Ag growth, the PANI membranes were washed by water thoroughly, and dried in air.

Superhydrophobic modification on Ag/PANI membranes

To make the Ag nanostructures hydrophobic, chemical modification of the Ag surface was carried out. In a typical experiment, the Ag/PANI substrates were firstly immersed into an ethanol solution of 0.1mol/L n-dodecyl mercaptan for 1 min. Then the substrates were taken out and rinsed thoroughly with ethanol and water, respectively. Afterwards, the chemically modified Ag/PANI substrates were dried in air before they could be used for SERS measurement.

Characterization

Scanning electron microscopy (SEM) images were taken on a FEI Inspect SEM. Static contact angles were measured by placing droplets of deionized water (0.2μL) on the surface. For SERS measurement, a droplet of methylene blue (MB) aqueous solution of different concentrations was placed on the substrate, and then dried in room temperature. The SERS spectra were recorded on a Renishaw In Via micro Raman spectroscopy system in a confocal Raman system (wavelength: 633 nm). For MB, spectra of samples were collected with a detection range from 600 to 1700 cm^{-1}.

Chemometrics Method

Prior to analysis, cosmic rays were removed from the spectra manually using a derivative filter. Background was removed by subtracting a fourth-order polynomial. All spectra were smoothed by a Savitzky–Golay algorithm with a third-order polynomial and a window size of 9 (points of window tells how many points to consider when looking at each individual point during the smoothing routine) using Origin 8.5. Data analysis was performed using partial least-squares (PLS) analysis. PLS was chosen from many chemometric techniques available because it only requires the concentrations of the analyte during calibration.[26, 27] Although the precise amount of analyte added to each sample is known in the experiments, the knowledge of the other chemicals in the background (e.g. acid and PANI signal from substrate preparation or impurities in the partition layers) was uncertain.

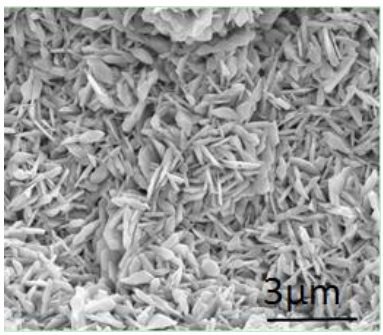

Fig. 1 SEM image of the as-fabricated Ag nanostructures grown on PANI membrane surface.

Prediction error in the calibration and validation sets was determined by calculating the root-mean-squared error of prediction (RMSEP)

$$\text{RMSEP}=\sqrt{\frac{\sum_1^n(conc_i-pred_i)^2}{n}} \quad (1)$$

In this equation, *conc* represents the actual log10 values of sample concentration, *pred* is the predicted log10 values of concentration for that sample, and *n* is the total number of samples. The number of PLS latent variables was optimized based on the lowest RMSEP values to avoid overfitting of spectral data. The correlation coefficient (R^2) and RMSEP were

used to evaluate the model. The higher the R^2 value or the lower RMSEP value is, the better predictability the model has.

Result and discussion

Morphology and wettability of the substrate

Fabrication of Ag Nanostructures on PANI membrane have been reported by our group previously.[25] Fig. 1 shows the SEM image of Ag nanostructures produced with lactic acid present in the $AgNO_3$ solutions. As mentioned,[28] with hydrazine treated PANI membrane and lactic acid present in $AgNO_3$ solutions, PANI film surface was fully covered by homogeneous Ag nanostructures that are assembled by thin Ag nanosheets. These nanosheets were densely arranged and overlapped. Therefore, concentrated hot spots and large electromagnetic enhancement can be expected on this substrate. After Ag nanosheets growth, the water contact angle on this substrate is about 44.95 ° (Fig. 2A), demonstrating that it is a hydrophilic substrate.

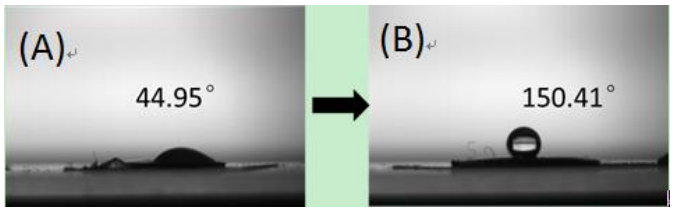

Fig. 2 Static contact angle on (A) as-fabricated Ag nanostructures and (B) n-dodecyl mercaptan modified Ag nanostructures.

Superhydrophobility is a phenomenon that a drop placed on a surface adopts a quasi-spherical shape with a contact angle greater than 150 °, rather than spreads over the plane of contact. After n-dodecyl mercaptan modification, the surface tension of the substrate can be greatly changed, and the contact angle θ of water droplets increased to 150.41 ° (Fig. 2B). This dramatic change of surface tension is a combination of geometric surface nanostructure and chemical modification, as flat surfaces may have a contact angle that is 120 ° at most *via* chemical modifications.[29] Superhydrophobic principles were proposed decades ago by Wenzel, Cassie and Baxter. [30, 31] Normally, superhydrophobility comes in two distinct flavours: a "sticky" surface on which liquid drops are difficult to move, and a "slippy" surface where there is little resistance to drop motion.[32] Therefore, to understand the superhydrophobic phenomenon of our substrate, it is necessary to know the specific mechanism. Fig. 3 shows that when a droplet of highly diluted solution is deposited on superhydrophobic substrate for evaporation, the drop will be highly fixed, which means the drop will reduce its volume without moving along the contact line. The observed contact angle on such a surface is given by Wenzel's equation:

$$\cos\theta_e^W = r\cos\theta_e \quad (2)$$

where the roughness r>1 is the ratio of the true surface area of the solid to its horizontal projection, and θ_e is the equilibrium contact angle on a smooth flat surface of the same material. When the liquid is in intimate contact with a microstructured surface, θ_e will change to θ_e^W. Based on Wenzel's equation, it is easy to explain the superhydrophobility of the as-fabricated substrate: after modifying the Ag nanostructure surface with n-dodecyl mercaptan, a low surface energy material, the roughness of Ag nanostructure can enhance the intrinsic wetting tendency of rolling up the liquid.

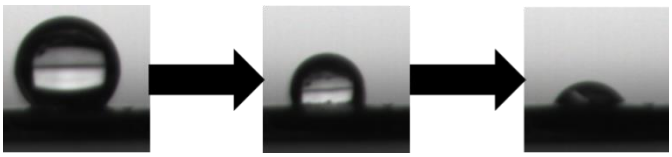

Fig. 3 Contact angle measurements during evaporation at three different stages.

Concentration effect of the superhydrophobic substrate

Nanoscale surface roughness of Ag structures can provide concentrated "hot spots" on the substrate, which significantly increases SERS enhancement. Moreover, after n-dodecyl mercaptan modification, the rough surface could exhibit superhydrophobility, which can dramatically reduce the contact area between the droplet and the underlying surface. Thus, the diluted analyte in the droplet can be highly concentrated after evaporation on the superhydrophobic surface for SERS detection. To quantitatively demonstrate the advantage of superhydrophobic SERS substrate in tracing small amount of molecules, a simplified model is established (Fig. 4). When two same droplets of extremely diluted solution are deposited on two different substrates, their contact areas with the substrate are different. To simplify the calculation, we assume that solution droplets are deposited uniformly on the substrates. Under this prerequisite, contact area is inversely proportional to number of molecules per unit area on the substrates. In addition, droplet may be assumed to be spherical, as the dominant force of sufficiently small droplets is the liquid-vapor surface tension and gravitation can be neglected.[33] The dimensionless Bond number (a measure of the importance of surface tension forces compared to body forces) can be consequently introduced as $B_o=\rho\times g\times R^2/\gamma_{LV}$, where ρ is the density of the liquid, R is the radius of the spherical drop prior to deposition on the surface, g is the acceleration due to gravity, and γ_{LV} is the liquid surface tension. When B_o<<1, gravitational effects vanish and the shape of the droplet may be assumed spherical everywhere.[34-36] For a drop of water with γ_{LV}=72.9 mJ/m^2, ρ=1000 kg/m^3, and diameter d=2R=1 mm, it can be calculated that B_o=~0.035, and thus the physics of micrometric or submillimetric drops is correctly governed by surface tension solely. Fig. 4A presents that on the hydrophilic substrate, the volume (V_1) and surface area (S_1) of the droplet can be:

$$V_1 = \pi R_1^3\left[\frac{4}{3} - (1-\cos\alpha_1)^2 + \frac{(1-\cos\alpha_1)^3}{3}\right] \quad (3)$$

$$S_1 = \pi R_1^2 \sin^2\alpha_1 \quad (4)$$

On the superhydrophobic substrate the volume (V_2) and surface area (S_2) of the droplet are:

$$V_2 = \pi R_2^3 * (1 - \cos\alpha_2)^2 * (2/3 + \cos\alpha_2/3) \quad (5)$$

$$S_2 = \pi R_2^2 \sin^2\alpha_2 \quad (6)$$

Since V_1=V_2, it can be deduced that

$$\frac{S_2}{S_1} = \left[\frac{\frac{4}{3} - (1-\cos\alpha_1)^2 + \frac{1}{3}(1-\cos\alpha_1)^3}{\frac{(1-\cos\alpha_2)^2(2+\cos\alpha_2)}{3}}\right]^{\frac{2}{3}} \quad (7)$$

As R_i is the radius of droplet and θ_i is the contact angle of corresponding situation, θ_2=180-α_2 and θ_1=α_1. For former situation, θ_2=150°,α_2=30 °,θ_1=45 °,α_1=45 °, therefore

$$\frac{S_2}{S_1} = \frac{1}{20.87} \quad (8)$$

It can be known now that simply by chemical modification the solution could be highly concentrated about 21 fold. To further substantiate this model, fluorescent image of 10^{-6} mol/L RhB was performed on the superhydrophobic substrate (Fig. 4C), which confirms that the diluted analyte in the droplet could be highly concentrated after evaporation.

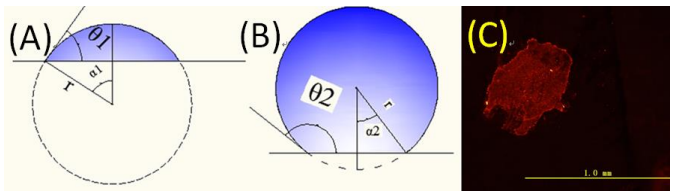

Fig. 4 Static contact angle images on (A) hydrophilic substrate and (B) superhydrophobic substrate. (C) Fluorescent image of Rhodamine B on the as-fabricated superhydrophobic substrate.

Comparison of SERS intensity on different substrates

To compare the SERS enhancement on superhydrophobic and hydrophilic substrates, 4 μL of MB aqueous solution with different concentrations from 10^{-4} to 10^{-8} mol/L were dropped on these substrates and dried in air. SERS spectrum of MB is dominated by C-C stretching at 1622cm^{-1}, and C–H in-plane ring deformation at 1398 cm^{-1}.[37-40] As shown in Fig. 5A, on the Ag nanostructures grown on PANI membrane, well-resolved Raman spectra of MB can be obtained at concentrations of 10^{-4} to 10^{-7} mol/L. Further decreasing the MB concentration to 10^{-8}mol/L makes the background noise comparable to the signal. However, after superhydrophobic modification, as shown in Fig. 5B, detection limit can reach as low as 10^{-8} mol/L. To demonstrate the wide applicability of our method, SERS performances on malic acid doped Ag/PANI substrate before and after superhydrophobic modification are also compared, as shown in Fig. 5C and D. On the Ag nanostructure grown on PANI membrane with the assistance of malic acid, MB can be tracked at a concentration higher than 10^{-5} mol/L. However, after superhydrophobic modification, the sensitivity is increased by 2 orders of magnitude, where MB with a concentration of 10^{-7} mol/L can be easily detected. Considering the calculated concentration factor of 21 as shown in Eq. 8, it is easy to explain the 1 or 2 order of magnitude improvement in detection limit. SERS sensitivity improvement of these substrates with different surface nanostructures after superhydrophobic modification indicates that this method can be a facile and effective method to further enhance the performance of SERS-active materials.

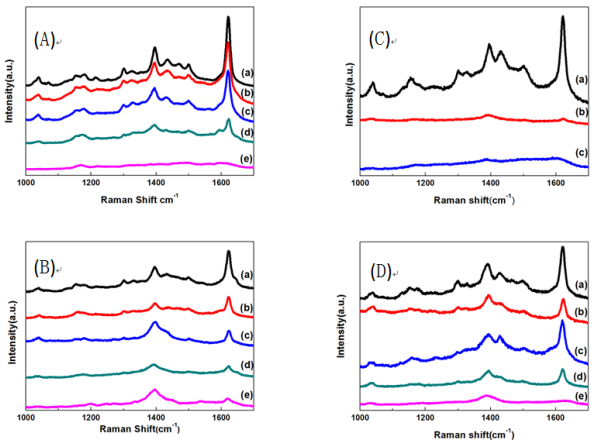

Fig. 5 SERS spectra of MB on lactic acid doped substrates: (A) hydrophilic substrates and (B) superhydrophobic substrates. SERS spectra of MB on malic acid doped substrates: (C)hydrophilic substrates and (D) superhydrophobic substrates. (a)10^{-4}, (b)10^{-5}, (c)10^{-6}, (d)10^{-7}, and (e)10^{-8} mol/L.

Reproducibility

The reproducibility of SERS response is a very important parameter for a SERS-active substrate. Usually, nanoparticle aggregates can produce large enhancement ability, but the signal reproducibility is poor. Therefore, self-assembled 2D nanoparticle films and 3D nanoparticle arrays have been developed as SERS substrate.[25] Our method to synthesize SERS-active substrate with the homogeneous Ag nanostructures fully covering PANI membrane surface is appealing, since the ordered nanostructures can endow these substrates with high enhancement ability and improved reproducibility. To test the reproducibility of our superhydrophobic substrates, the SERS spectra of 10^{-4} mol/L MB were collected from 22 random sites. As can be seen in Fig. 6, well discernible SERS spectra of MB with similar intensity are obtained at all sites. For the strongest peak at 1622 cm^{-1}, the relative standard deviation (RSD) of SERS intensity at 22 different sites on the same substrate is about 14.2%, which is comparable to previous reports (11%).[41] This low RSD indicates the structure and surface property of the superhydrophobic substrate is relatively uniform, which is important to generate reproducible SERS signals over the surface.

Quantitative detection

Although SERS performance of our substrate is in the relatively low sensitivity regime as compared to that obtained on some reported substrates, but their SERS signals typically show fluctuations in intensity (blinking), band positions, etc.[42] Observed signal from our substrate is composed of

contributions from numerous scattering molecules, and an average effect leads to much more stable and reproducible responses (RSD=14.2%). Here, we investigated the feasibility of using the SERS-active superhydrophobic substrate for quantitative detection. A PLS calibration model was built using 68 independent spectra of known concentrations of MB (10^{-4}~10^{-6} mol/L). It has been reported that PLS model using data collected from a single point presents great improvement in accuracy, but predictions perform poorly when applied to data collected from different focal points.[43, 44] To better simulate practical application of our substrate rather than "in lab-only" prediction, a versatile and robust mathematical model is built using data collected from different locations.

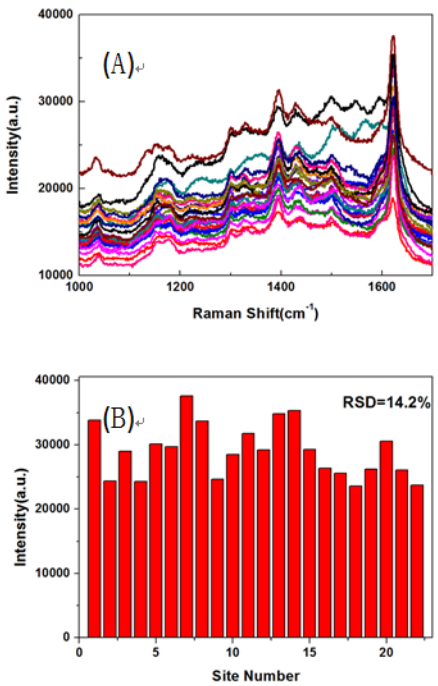

Fig. 6 (A) SERS spectra of 10^{-4} mol/L MB collected from 22 random sites. (B) The SERS intensities of the strongest peak (1622 cm^{-1}) at 22 sites and the calculated RSD.

The interaction of analytes and SERS-active substrate has been further analyzed by fitting the curve with Hill equation. Generally, the SERS intensity (I_{SERS}) is proportional to the surface coverage of adsorbed molecules on hot spots (Θ), assuming all hot spots are uniform over the surface, and the surface coverage follows the Hill equation,[12]

$$I_{SERS} = C\Theta = C\frac{c^n}{k^n + c^n} \quad (9)$$

where C is a constant, c is the concentration of the solution, k is the equilibrium constant for dissociation, and n is a cooperative constant. We found that at MB concentrations above 10^{-3} mol/L, the SERS intensity reached a plateau, indicating the adsorption of the molecules was saturated the surfaces. At lower concentrations, where $c \ll k$, $\log I_{SERS} \approx n\log c + \text{const}$. We compared the PLS models built by original dataset and log 10 values of dataset and found that after log transformation, the dataset would be more reliable for quantitative analysis of MB at low concentrations.

The number of latent variables can be interpreted as inherent dimensionality of the system. These variables can include, and are not limited to, concentration of the analyte, temperature and humidity conditions in the laboratory on the day of the experiment, the focusing of the optical elements, the enhancement of the sensing surface at different locations, the laser power and mode fluctuations, as well as noise in the data. Using too many latent variables can cause overmodeling of the data, including all the above-mentioned variation in the experimental design to build a robust calibration model. Based on calibration, 95.1% of the data is represented by five latent variables, namely correlation coefficient R^2=95.1%. Here, the use of five latent variables and log transformation resulted in a model with a root mean square error of estimation (RMSEE) of 0.130 (Fig. 7). The RMSEE describes the accuracy of the model itself. A low RMSEE is necessary for, but does not ensure, accurate prediction of concentrations based on measurements from samples outside the training set. Therefore, a separate set of spectra consisting of 32 independent data points was used to validate the model. Validation tests the ability of the model to predict the concentration of samples not used in the calibration, and more precisely reflects the accuracy of the substrate. The RMSEP was calculated to be 0.226. These results indicate that the superhydrophobic Ag/PANI substrate is capable of making acceptably accurate concentration measurements even with a diverse sample population.

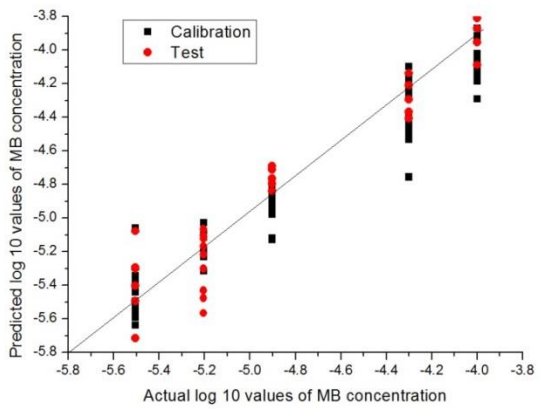

Fig. 7 Prediction/validation plots using multiple locations on substrate. PLS calibration plots were constructed using 68 data points taken over a range of concentrations (10^{-4}~10^{-6} mol/L) from different locations on Ag/PANI substrate. Five latent variables were used to generate the mathematical model, which has an RMSEE=0.130175. The central line represents the ideal prediction axis, not a best-fit curve. An independent test set with 32 data points was used to test the predictive capability of the mathematical model. RMSEP=0.226, R^2=95.1%.

Conclusions

We have successfully fabricated a superhydrophobic substrate based on n-dodecyl mercaptan modified Ag nanostructures grown on PANI membrane with the assistance of lactic acid for SERS application. In addition to the high enhancement from Ag nanostructures, the condensation effect of the superhydrophobic surface could further amplify the SERS signal to achieve more sensitive detection. The developed superhydrophobic substrate with high signal reproducibility has been successfully used for SERS quantitative detection of a target molecule, methylene blue (MB). Validation of the PLS model with 32 independent measurements yields an RMSEP of 0.226, R^2 of 95.1%. The present study may provide new insight in fabricating efficient substrate for SERS and it is expected that this superhydrophobic substrate can be widely used in the trace analysis due to the facile synthesis method and high performance in SERS.

Acknowledgements

We thank support from NSFC (No.21471039, 21203045, 21101041, 21003029, 91122002), Fundamental Research Funds for the Central Universities (No. HIT.NSRIF.2010065 and 2011017, and HIT.BRETIII. 201223), and Open Project of State Key Laboratory of Urban Water Resource and Environment, Harbin Institute of Technology (No. ES201411).

Notes and references

Department of Chemistry, Harbin Institute of Technology, Harbin 150001, China. Email: pxu@hit.edu.cn; hanxijiang@hit.edu.cn

1. K. Kneipp, *Physics Today*, 2007, **60**, 40-46.
2. M. T. Sun, Z. L. Zhang, P. J. Wang, Q. Li, F. C. Ma and H. X. Xu, *Light-Sci Appl*, 2013, **2**, e112.
3. J. F. Li, Y. F. Huang, Y. Ding, Z. L. Yang, S. B. Li, X. S. Zhou, F. R. Fan, W. Zhang, Z. Y. Zhou, D. Y. Wu, B. Ren, Z. L. Wang and Z. Q. Tian, *Nature*, 2010, **464**, 392-395.
4. X. H. Li, G. Y. Chen, L. B. Yang, Z. Jin and J. H. Liu, *Advanced Functional Materials*, 2010, **20**, 2815-2824.
5. X. Wang, X. M. Qian, J. J. Beitler, Z. G. Chen, F. R. Khuri, M. M. Lewis, H. J. C. Shin, S. M. Nie and D. M. Shin, *Cancer Research*, 2011, **71**, 1526-1532.
6. R. G. Freeman, K. C. Grabar, K. J. Allison, R. M. Bright, J. A. Davis, A. P. Guthrie, M. B. Hommer, M. A. Jackson, P. C. Smith, D. G. Walter and M. J. Natan, *Science*, 1995, **267**, 1629-1632.
7. L. Jiang, T. T. You, P. G. Yin, Y. Shang, D. F. Zhang, L. Guo and S. H. Yang, *Nanoscale*, 2013, **5**, 2784-2789.
8. A. Musumeci, D. Gosztola, T. Schiller, N. M. Dimitrijevic, V. Mujica, D. Martin and T. Rajh, *Journal of the American Chemical Society*, 2009, **131**, 6040-+.
9. L. L. Sun, Y. H. Song, L. Wang, C. L. Guo, Y. J. Sun, Z. L. Liu and Z. Li, *J Phys Chem C*, 2008, **112**, 1415-1422.
10. S. C. Xu, Y. X. Zhang, Y. Y. Luo, S. Wang, H. L. Ding, J. M. Xu and G. H. Li, *Analyst*, 2013, **138**, 4519-4525.
11. J. W. Zheng, X. W. Li, R. N. Gu and T. H. Lu, *Journal of Physical Chemistry B*, 2002, **106**, 1019-1023.
12. A. Kim, S. J. Barcelo, R. S. Williams and Z. Y. Li, *Analytical Chemistry*, 2012, **84**, 9303-9309.
13. M. Mulvihill, A. Tao, K. Benjauthrit, J. Arnold and P. Yang, *Angewandte Chemie-International Edition*, 2008, **47**, 6456-6460.
14. X. M. Qian and S. M. Nie, *Chemical Society Reviews*, 2008, **37**, 912-920.
15. H. K. Lee, Y. H. Lee, Q. Zhang, I. Y. Phang, J. M. R. Tan, Y. Cui and X. Y. Ling, *Acs Appl Mater Inter*, 2013, **5**, 11409-11418.
16. F. De Angelis, F. Gentile, F. Mecarini, G. Das, M. Moretti, P. Candeloro, M. L. Coluccio, G. Cojoc, A. Accardo, C. Liberale, R. P. Zaccaria, G. Perozziello, L. Tirinato, A. Toma, G. Cuda, R. Cingolani and E. Di Fabrizio, *Nature Photonics*, 2011, **5**, 683-688.
17. W. Barthlott and C. Neinhuis, *Planta*, 1997, **202**, 1-8.
18. K. S. Liu, X. Yao and L. Jiang, *Chemical Society Reviews*, 2010, **39**, 3240-3255.
19. M. Rycenga, C. M. Cobley, J. Zeng, W. Y. Li, C. H. Moran, Q. Zhang, D. Qin and Y. N. Xia, *Chemical Reviews*, 2011, **111**, 3669-3712.
20. J. Henzie, S. C. Andrews, X. Y. Ling, Z. Y. Li and P. D. Yang, *Proceedings of the National Academy of Sciences of the United States of America*, 2013, **110**, 6640-6645.
21. P. Xu, X. J. Han, B. Zhang, Y. C. Du and H. L. Wang, *Chem Soc Rev*, 2014, **43**, 1349-1360.
22. P. Xu, B. Zhang, N. H. Mack, S. K. Doorn, X. J. Han and H. L. Wang, *J Mater Chem*, 2010, **20**, 7222-7226.
23. J. Yan, X. J. Han, J. J. He, L. L. Kang, B. Zhang, Y. C. Du, H. T. Zhao, C. K. Dong, H. L. Wang and P. Xu, *Acs Appl Mater Inter*, 2012, **4**, 2752-2756.
24. R. N. Wenzel, *Industrial & Engineering Chemistry*, 1936, **28**, 988-994.
25. P. Xu, N. H. Mack, S. H. Jeon, S. K. Doorn, X. J. Han and H. L. Wang, *Langmuir*, 2010, **26**, 8882-8886.
26. P. Geladi and B. R. Kowalski, *Analytica Chimica Acta*, 1986, **185**, 1-17.
27. D. M. Haaland and E. V. Thomas, *Analytical Chemistry*, 1988, **60**, 1193-1202.
28. J. J. He, X. J. Han, J. Yan, L. L. Kang, B. Zhang, Y. C. Du, C. K. Dong, H. L. Wang and P. Xu, *Crystengcomm*, 2012, **14**, 4952-4954.
29. G. Shafrin Elaine and A. Zisman William, in *Contact Angle, Wettability, and Adhesion*, AMERICAN CHEMICAL SOCIETY, 1964, vol. 43, pp. 145-157.
30. A. B. D. Cassie and S. Baxter, *Transactions of the Faraday Society*, 1944, **40**, 546-551.
31. E. Johnson Rulon and H. Dettre Robert, in *Contact Angle, Wettability, and Adhesion*, AMERICAN CHEMICAL SOCIETY, 1964, vol. 43, pp. 112-135.
32. D. Quere, A. Lafuma and J. Bico, *Nanotechnology*, 2003, **14**, 1109-1112.
33. G. McHale, N. J. Shirtcliffe and M. I. Newton, *Analyst*, 2004, **129**, 284-287.
34. P. Aussillous and D. Quere, *Nature*, 2001, **411**, 924-927.
35. R. Blossey, *Nature Materials*, 2003, **2**, 301-306.
36. L. Mahadevan and Y. Pomeau, *Physics of Fluids*, 1999, **11**, 2449-2453.
37. S. W. Li, P. Xu, Z. Q. Ren, B. Zhang, Y. C. Du, X. J. Han, N. H. Mack and H. L. Wang, *Acs Appl Mater Inter*, 2013, **5**, 49-54.
38. S. W. Li, L. Xiong, S. Liu and P. Xu, *Rsc Adv*, 2014, **4**, 16121-16126.
39. L. L. Kang, P. Xu, D. T. Chen, B. Zhang, Y. C. Du, X. J. Han, Q. Li and H. L. Wang, *J Phys Chem C*, 2013, **117**, 10007-10012.

40. S. H. D. Nicolai, P. R. P. Rodrigues, S. M. L. Agostinho and J. C. Rubim, *J Electroanal Chem*, 2002, **527**, 103-111.
41. F. G. Xu, Y. Zhang, Y. J. Sun, Y. Shi, Z. W. Wen and Z. Li, *J Phys Chem C*, 2011, **115**, 9977-9983.
42. S. E. J. Bell and N. M. S. Sirimuthu, *Chemical Society Reviews*, 2008, **37**, 1012-1024.
43. D. A. Stuart, C. R. Yonzon, X. Y. Zhang, O. Lyandres, N. C. Shah, M. R. Glucksberg, J. T. Walsh and R. P. Van Duyne, *Analytical Chemistry*, 2005, **77**, 4013-4019.
44. C. R. Yonzon, C. L. Haynes, X. Y. Zhang, J. T. Walsh and R. P. Van Duyne, *Analytical Chemistry*, 2004, **76**, 78-85.